crystals

MDPI

Article

The Role of Boron Addition on Solidification Behavior and Microstructural Evolution of a High Niobium-Containing TiAl Alloy

Fan Zhang [1], Zeen Wu [1,*], Xiaoye Wang [1], Tiebang Zhang [2], Yongchun Zhang [1] and Qiao Li [3]

[1] Shannxi Key Laboratory of Advanced Manufacturing and Evaluation of Robot Key Components, Baoji University of Arts and Sciences, Baoji 721016, China; zhangfan0903@163.com (F.Z.); xiaoyewang221@163.com (X.W.); yongchun01234@163.com (Y.Z.)
[2] State Key Laboratory of Solidification Processing, Northwestern Polytechnical University, Xi'an 710072, China; tiebangzhang@nwpu.edu.cn
[3] Baoji Ti-Price Anode Co., Ltd., Baoji 710072, China; lq@anode.cc
* Correspondence: zeen0907@163.com; Tel.: +86-091-7336-4295; Fax: +86-091-7336-8955

Abstract: This work investigates the role of boron addition in the solidification behavior and microstructural evolution during the heat treatment process of Ti-46Al-8Nb-*x*B (x = 0.1, 0.7, 1.4, 2.5 at.%). The results show that the solid solution boron element prefers to occupy the interstitial vacancies of the α_2 phase in the alloy. However, the solid solubility of the boron element in high Nb-containing TiAl alloys is extremely low. Therefore, it does not have a significant effect on the lattice distortion of α_2 and γ phases in the alloy. When the boron content is added up to 0.1%, a B27-type TiB precipitated phase is produced in the alloy. The morphology of borides mostly shows short rod-like structures, and a few show long curved shapes. And the addition of boron refines both the alloy colony size and the lamellar structure. Furthermore, it is also found that boron addition weakens the casting texture of the alloy. After a solid solution and different time aging heat treatment process, the microstructure of different boron content alloys have experienced obvious coarsening phenomenon. However, the morphology of the boride is closely related to boron content and heat treatment.

Keywords: high Nb-containing TiAl alloy; boron; microstructural evolution; heat treatment

Citation: Zhang, F.; Wu, Z.; Wang, X.; Zhang, T.; Zhang, Y.; Li, Q. The Role of Boron Addition on Solidification Behavior and Microstructural Evolution of a High Niobium-Containing TiAl Alloy. *Crystals* **2023**, *13*, 1494. https://doi.org/10.3390/cryst13101494

Academic Editor: Vladimir I. Zverev

Received: 19 September 2023
Revised: 7 October 2023
Accepted: 12 October 2023
Published: 14 October 2023

1. Introduction

TiAl alloys have great potential for applications in the aerospace and automotive industries, as well as in nuclear energy, due to their excellent all-around performance [1–4]. However, the large-scale application of TiAl alloys is still limited by many aspects, the most prominent of which is their brittleness [5]. The room temperature intrinsic brittleness, poor molding ability, and high temperature oxidation resistance of TiAl alloys are serious obstacles to their practical application in various important fields [6,7]. Therefore, how to improve the intrinsic brittleness of TiAl alloys and enhance the microstructural stability of the alloys in service is one of the bottlenecks that need to be solved in the application of TiAl alloys.

At present, the most direct and effective way is to introduce the second phase for toughening by alloying or compositing methods to form a multilevel and multiscale microstructure in alloys [8], which in turn exhibits excellent comprehensive performance. Therefore, in this work, the microalloying of TiAl alloys will be investigated. It has been found that TiAl alloys with single β solidification have significantly weakened columnar crystal features in the microstructure, resulting in refinement microstructure and reduced segregation [9,10]. Therefore, the aluminum content should not be too high for TiAl alloys [11]. As for the alloying process, for Nb alloying and the development of high Nb-containing TiAl alloys, compared with ordinary TiAl alloys, its service temperature can

be increased by 60~100 °C, the high-temperature yield strength is doubled and the high-temperature oxidation resistance is also greatly improved [12,13]. In addition, the addition of the Nb element can reduce the stacking fault energy of γ phase in TiAl alloy, which is conducive to the opening of deformation twins, thereby reducing the room temperature brittleness of the alloy [14]. Therefore, high Nb-containing TiAl alloys with excellent high-temperature performance have received extensive attention from scholars, among which β-solidified high Nb-containing TiAl alloys have become one of the hot directions of research. In this work, the alloy composition of high Nb-containing TiAl alloy with β-solidification condition is selected as the research object.

On the selection of micro-alloying elements, it is found that scholars generally choose the transition group metal elements. However, the micro-alloying of transition group elements is not conducive to the weight reduction design concept of TiAl alloys on the one hand, and is also prone to compositional segregation in the casting process. In recent years, lightweight nonmetallic elements, which have a significant effect on both the microstructure and properties of alloys, have received more and more attention [15,16]. Studies have shown that borides can refine the colony size of TiAl alloy lamellar and improve the room temperature mechanical properties of the alloy [17,18]. Meanwhile, the different morphologies and contents of borides have great influence on the microstructure evolution and mechanical properties of TiAl alloy [19,20]. However, the current studies on the role of B are mostly in binary TiAl alloys. The role of boron in high Nb-containing TiAl alloys, especially in β-solidified high Nb-containing TiAl alloys which have a great potential for application, has not been well studied. There are fewer related studies at present. Therefore, it is necessary to investigate the boride addition to β-solidified high Nb-containing TiAl alloys on the alloy microstructural evolution, as well as the evolutionary behavior of borides during heat treatment. In this work, the role of boron addition on the solidification behavior and microstructural evolution during the heat treatment process of a β-solidified high Nb-containing TiAl alloy have been investigated. Through this work, it is expected to improve the comprehensive performance of the selected alloys and provide theoretical guidance for the engineering application of lightweight and high-strength TiAl alloys.

2. Experimental Procedures

In this work, the composition of the experimental alloys were Ti-46Al-8Nb-*x*B (x = 0, 0.1, 0.7, 1.4, 2.5 at.%). According to vertical sections close to the Al-Ti side of Al-Nb-Ti system [21], β phase is the solidification initial phase of the selected alloy. Therefore, the experimental alloy is a β-solidified high Nb-containing TiAl alloy. Each ingot was prepared under argon protection in a vacuum non-consumable arc melting furnace. The raw materials used for the experimental alloy melting were high purity titanium sponge (99.99 wt.%), high purity aluminum (99.99 wt.%) and titanium–niobium binary alloy (52.47 wt.% niobium content). Boron was brought in as TiB_2 (99.8 wt%) intermediate alloy powder. Each ingot was re-melted 5 times to guarantee the homogenization of the alloy composition. After melting, each ingot was weighed. Calculations showed that the weight loss per ingot was less than 0.1 wt.% and therefore the alloy composition was considered to be the design composition. Ingots with boron content of 0.7, 1.4 and 2.5% were selected for heat treatment. The specimens were first placed in a vacuum heat treatment furnace and heated up to 1380 °C under argon protection for 1 h of solution treatment and then quenched in water at room temperature. After water quenching, the specimen alloys were aged at 900 °C for 3–24 h.

The phase composition of the samples was determined by X-ray diffraction (XRD) (Panalytical, Almelo, Holland) with Cu *K*α radiation (λ = 1.54056 Å). The samples were scanned over a range of 20–90° with a scan rate of 0.05° s^{-1}. Scanning electron microscopy (SEM) (Tescan, Brno, Czech Republic) was used to analyze the microstructure of the alloy. Elemental distribution and composition of precipitated phases in the alloy were analyzed by electron probe microanalyzer (EPMA) (SHIMADZU, Kyoto, Japan). In order to determine the weaving and crystallographic information in the alloy, electron backscatter diffraction

(EBSD) (OXFORD INSTRUMENTS, Oxford, UK) was performed in the central region of the sample at an accelerating voltage of 20 kV. Furthermore, the microstructure and precipitated phases of the alloy were analyzed using transmission electron microscopy (TEM) (FEI, Hillsborough, America). Specimens for SEM view were prepared by standard metallographic polishing procedures using a modifying Kroll etching solution. The etching solution consisted of H_2O: HNO_3: HF in a ratio of 8:1:1. Preparation of TEM observation foils was carried out by ion milling method. The solid solution stage adopts a stepped heating process, with a heating rate of 10 K/min from room temperature to 800 °C, and a 5 K/min from 800 °C to 1380 °C. The aging stage also employs a stepped heating method, with a heating rate of 5 K/min from room temperature to 500 °C, and a 3 K/min from 500 °C to 900 °C.

3. Results and Discussion

3.1. Phase Composition

Figure 1 illustrates the XRD patterns of Ti-46Al-8Nb-*x*C (x = 0, 0.1, 0.7, 1.4, 2.5%). According to the phase diagram [21], the phase composition of Ti-46Al-8Nb alloy is γ and α_2. As can be seen from the figure, diffraction peaks of the γ and α_2 phases are detected in the Ti-46Al-8Nb alloy, but diffraction peaks of the Nb compounds are not detected. However, the element Nb is not present in a solid solution form in the interstitial vacancies of γ and α_2, but replaces Ti-sites within the Ti-sublattice [22]. Therefore, according to the crystal structure, Nb elements are present in the lattice sites of both the α_2 and γ phases. With the addition of 0.1% B, the main diffraction peaks do not change, and the alloy still consisted of γ and α_2 phases. By further increasing the boron content to 0.7%, in addition to the two main peaks γ and α_2, diffraction peaks of a new phase TiB phase are developed in the alloy. This indicates that the elemental B content has exceeded its solid solubility in the alloy and thus exists as a precipitated phase. Therefore, the solid solubility of boron in the Ti-46Al-8Nb alloy is less than 0.7%. When increasing the boron content to 1.4 and 2.5%, the diffraction peaks of the TiB phase are more obvious, indicating that its content is gradually increasing. Since the borides are TiB phases, the Ti atoms are consumed during its reformation. Therefore, the content of the α_2 phase is gradually decreasing in the alloy. This can be proved by the fact that the diffraction peaks intensity of the α_2 phase in Figure 1 is gradually decreasing.

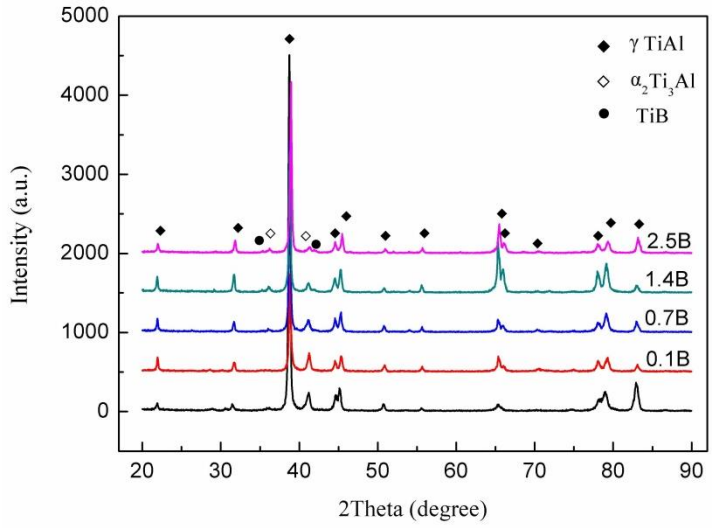

Figure 1. X-ray diffraction patterns of Ti-46Al-8Nb-*x*B (x = 0, 0.1, 0.7, 1.4, 2.5 at.%).

The evolution of lattice parameters and unit cell volume of the (a) γ and (b) α_2 phases as a function of boron content are displayed in Figure 2. For the γ phase, its cell volume is elevated at a boron addition of 0.1%. It indicates that element B is present in solid solution form in the γ phase, which in turn results in lattice distortion. As the boron content

continues to increase, the cell volume of the γ phase no longer changes, although the lattice parameters *a* and *c* change slightly. This suggests that the solid solution limit of boron in the γ phase is less than 0.1%. For the α_2 phase, the lattice changes are basically the same as for the γ phase. Its cell volume increases at a boron addition of 0.1%. As the boron content continues to increase, its cell volume no longer changes. This indicates that the solid solution limit of boron in the α_2 phase is also lower than 0.1%.

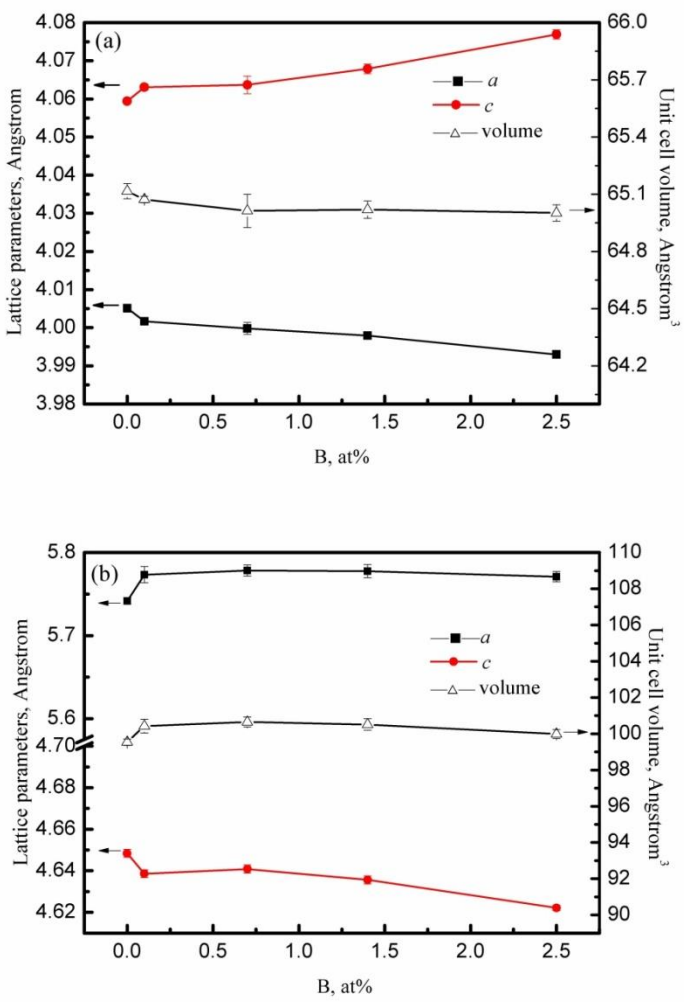

Figure 2. Evolution of lattice parameters and unit cell volume of (**a**) γ and (**b**) α_2 phases as a function of boron content.

By the analysis of Figure 2, the solid solution limit of the boron element in the alloy should be less than 0.1%. However, in the XRD test in Figure 1, the presence of borides is not detected when the boron content is 0.1%. This may be due to the accuracy of XRD, which fails to detect the presence of borides at low boron content. According to previous research results, the solid solubility of interstitial atoms in the α_2 phase is much higher than that in the γ phase [16,23]. This is mainly because interstitial atoms prefer to occupy octahedral sites of "Ti6 type" in the $D0_{19}$ structure of the α_2 phase [22,24]. However, in the present work, there is no significant difference in the solid solubility of elemental boron in the α_2 and γ phases. This is mainly due to the nature of the element boron, which prefers to combine with Ti atoms [25]. Elemental boron is easy to combine with Ti atoms to form compounds, which in turn leads to its lower solid solubility.

3.2. Microstructural Characterization

The SEM images of the as-cast Ti-46Al-8Nb-*x*B (*x* = 0, 0.1, 0.7, 1.4, 2.5%) are shown in Figure 3. It can be seen that the morphology of as-cast Ti-46Al-8Nb is a coarse equiaxial

crystal microstructure, and white β phase remaining in the matrix. When 0.1% B is added, the β phase in the microstructure of the alloy disappears, but the morphology of as-cast Ti-46Al-8Nb-0.1B is still considered to be a coarse equiaxial crystal microstructure. Meanwhile, a small number of boride precipitates are found to exist in the alloy. Combined with XRD analysis, the precipitated boride is TiB, which further illustrates that the solid solubility of B in the alloy is less than 0.1%. When the B element content is low, the low concentration of B atoms tends to diffuse in the liquid phase in front of the solidification boundary, making enrichment difficult. As a result, the concentration of the TiB heterogeneous nucleation matrix is low and the nucleation rate cannot be effectively improved [26]. Therefore, the lower content of the B element fails to effectively refine the microstructure of the alloy.

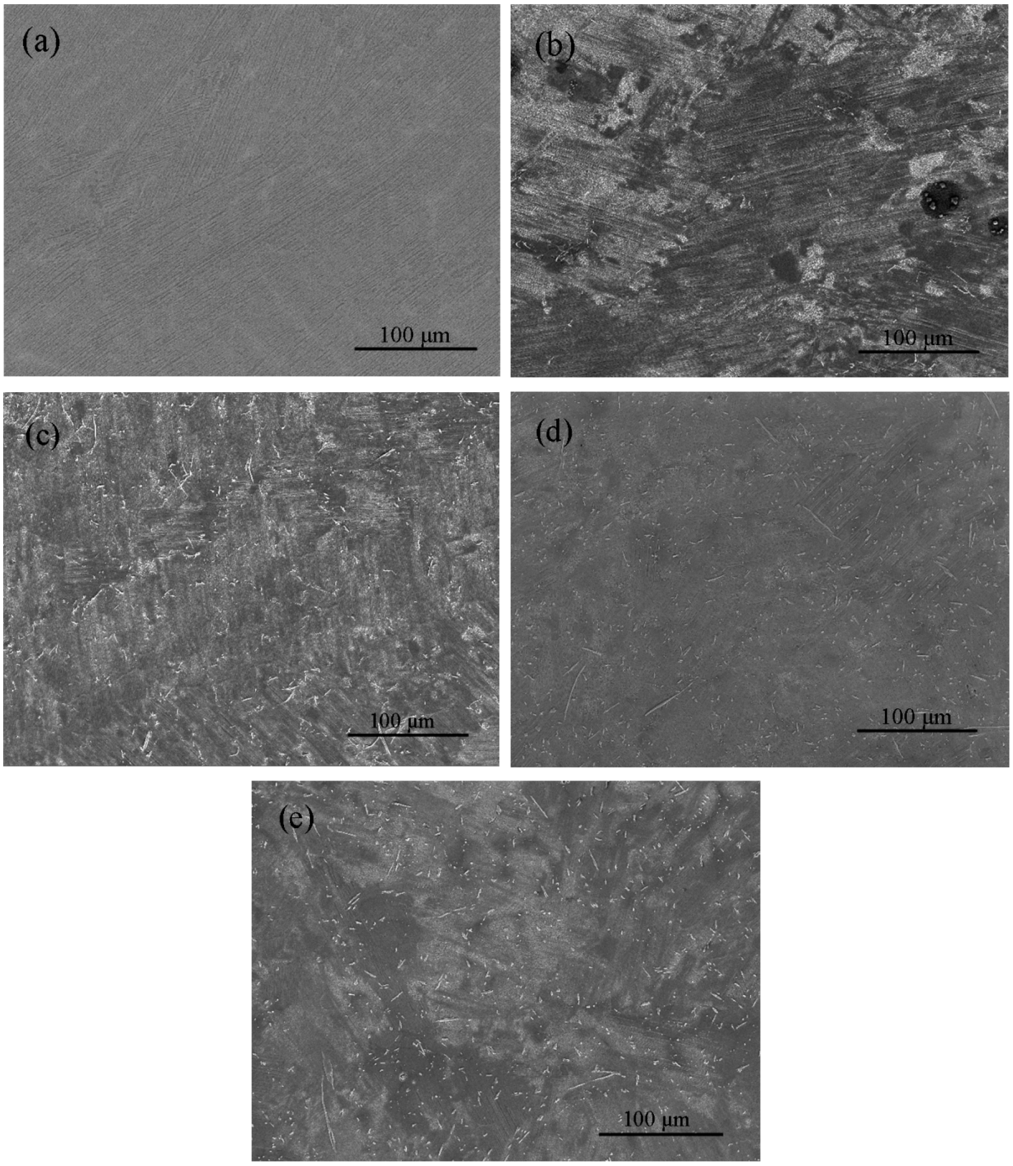

Figure 3. The SEM images of the as-cast Ti-46Al-8Nb-*x*B: (**a**) $x = 0$; (**b**) $x = 0.1$; (**c**) $x = 0.7$; (**d**) $x = 1.4$; (**e**) $x = 2.5$.

With the addition of boron content to 0.7 or more, the microstructure of the alloy is significantly and continuously refined, and the content of borides in the alloy gradually increases. It has been suggested that sufficient boron content along the solidification front is a key condition for grain refinement [27]. There are two reasons why the addition of high levels of boron significantly refines the alloy microstructure. Firstly, as the B content increases, a large number of B atoms are discharged into the melt in front of the solidification

boundary, and the enrichment of B atoms aggravates the constitutional undercooling [17]. As the solidification process proceeds, a large amount of primary TiB phase precipitates in the dendritic region of the β phase, providing more nucleation cores for the α phase. Secondly, due to the low solubility of boron in solids, it is expelled into the liquid before solidification. As more and more new grains are formed, the boron solubility at the front of the solidified liquid phase again reaches the critical concentration [28]. This in turn causes precipitation of new TiB phases, which further provide heterogeneous nucleation sites for the α phase.

It has been suggested that the morphology of borides is related to the boron content [29]. As shown in Figure 3, no significant change in the morphology of borides in the alloy was observed with the increase in boron content. The morphology of borides is dominated by short rods and granules, and a few morphologies are curly and long.

Figure 4 shows the compositional distribution of Ti-46Al-8Nb-1.4B obtained by EPMA analysis. Figure 4a shows the detection position of EPMA, including two borides, components 1 and 2, and the black line is the composition scanning line. Boride composition data are shown in Table 1. As can be seen in Figure 4a, the fluctuations of Ti and Al elements are approximately uniform when the compositional scanning line passes through the lamellar colonies. The reason is that the lamellar colonies are composed of an Al rich γ phase and Ti rich α_2 phase arranged in intervals. When the compositional scanning line passes through the borides, the fluctuations of several elements are different, with a sharp decrease in the content of Al and a significant increase in Nb, and the fluctuations of Nb are opposite to those of Ti. The results in Table 1 explain this phenomenon. As can be seen from Table 1, the Al content in the borides is low, and therefore show a sharp decrease on the composition line scanning. From the previous analysis, it is clear that Nb replaces the Ti-site in the lattice. Therefore, in boride TiB, Ti and Nb can be replaced with each other. As a result, the relationship between the two elements changes to the opposite. As can be seen from Table 1, the sum of Nb and Ti content is comparable to the content of the B element, which is basically consistent with the ratio of Ti:B as 1:1, which can also confirm this explanation. It is also known that the boride phase in the high Nb-containing TiAl alloy is a Nb-rich phase.

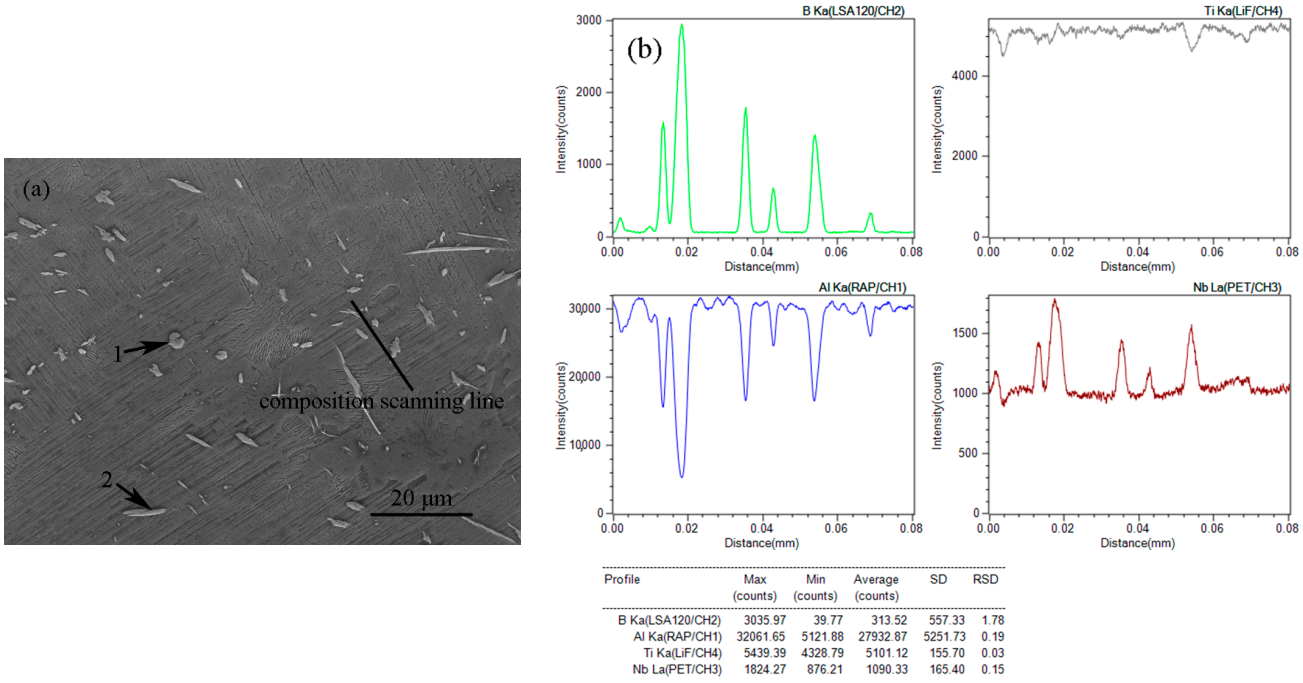

Profile	Max (counts)	Min (counts)	Average (counts)	SD	RSD
B Ka(LSA120/CH2)	3035.97	39.77	313.52	557.33	1.78
Al Ka(RAP/CH1)	32061.65	5121.88	27932.87	5251.73	0.19
Ti Ka(LiF/CH4)	5439.39	4328.79	5101.12	155.70	0.03
Nb La(PET/CH3)	1824.27	876.21	1090.33	165.40	0.15

Figure 4. Compositional distribution of Ti-46Al-8Nb-1.4B obtained by EPMA analysis: (**a**) detection position of EPMA, 1 and 2 arrows indicate the detection positions of the two borides; (**b**) shows the compositional distribution of the line scan in Figure 4a.

Table 1. EPMA data for points 1 and 2 in Figure 4a.

Data	Al Ka	B Ka	Nb La	Ti Ka	Total
	At%	At%	At%	At%	At%
1	10.13	45.398	9.263	35.209	100
2	8.029	46.468	10.497	35.007	100

Figure 5 presents the TEM images of Ti-46Al-8Nb, Ti-46Al-8Nb-2.5B and boride in Ti-46Al-8Nb-2.5B alloy with the corresponding SAED pattern. By comparing Figure 5a,b, it indicates that both α_2 and γ phases within the lamellar in the alloy are significantly refined after the addition of 2.5% B. It is clear from the previous analysis that boron addition significantly refines the lamellar colony of the alloy. Therefore, it can be concluded that the addition of boron can simultaneously refine the lamellar colony and lamellar microstructure of the alloy. According to the literature, four main titanium boride phases are present in TiAl alloys, namely TiB (B27), TiB (B_f), TiB_2 (C32) and Ti_3B_4 (D7b) [30]. The lattice structure of the boride phases is more related to the alloy composition. Studies have shown that low Al and high Nb content are beneficial for the precipitation of a B27-structured TiB phase [30,31]. As shown in Figure 5c,d, the boride in this experiment is a TiB phase with a B27 structure. Since the experimental alloy is a low Al and high Nb alloy, the present work also confirms the previous statement.

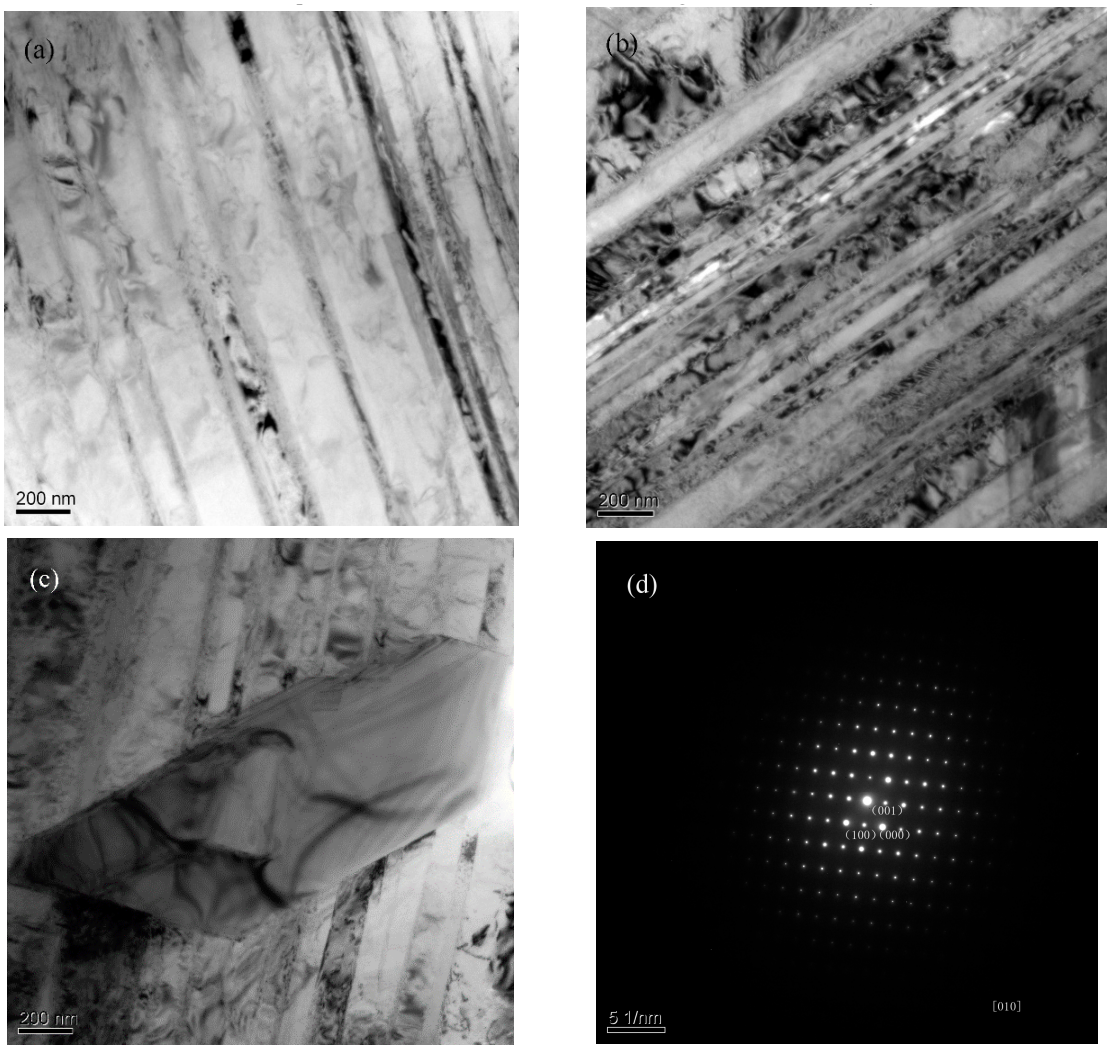

Figure 5. TEM images of (**a**) Ti-46Al-8Nb, (**b**) Ti-46Al-8Nb-2.5B, (**c**) boride in Ti-46Al-8Nb-2.5B and (**d**) the corresponding SAED pattern of the boride.

Figure 6 gives the pole figures of γ, α_2 and TiB phases in Ti-46Al-8Nb-2.5B obtained by EBSD. This is mainly to detect the casting texture in the alloy. As can be seen from the figure, the grain orientations of the γ, α_2 and TiB phases are all random in the {100}, {110}, and {111} orientations, with no obvious casting texture present. This suggests that B addition weakens the casting texture of the alloy. It has been reported that this is mainly due to the presence of the boride phase [29]. From the previous analysis, it is clear that borides can become heterogeneous nucleation sites. And the α phase produced by the heterogeneous nucleation points destroys the strict Bragg orientation relationship during the phase transition. As a result, the casting texture in the alloy is weakened.

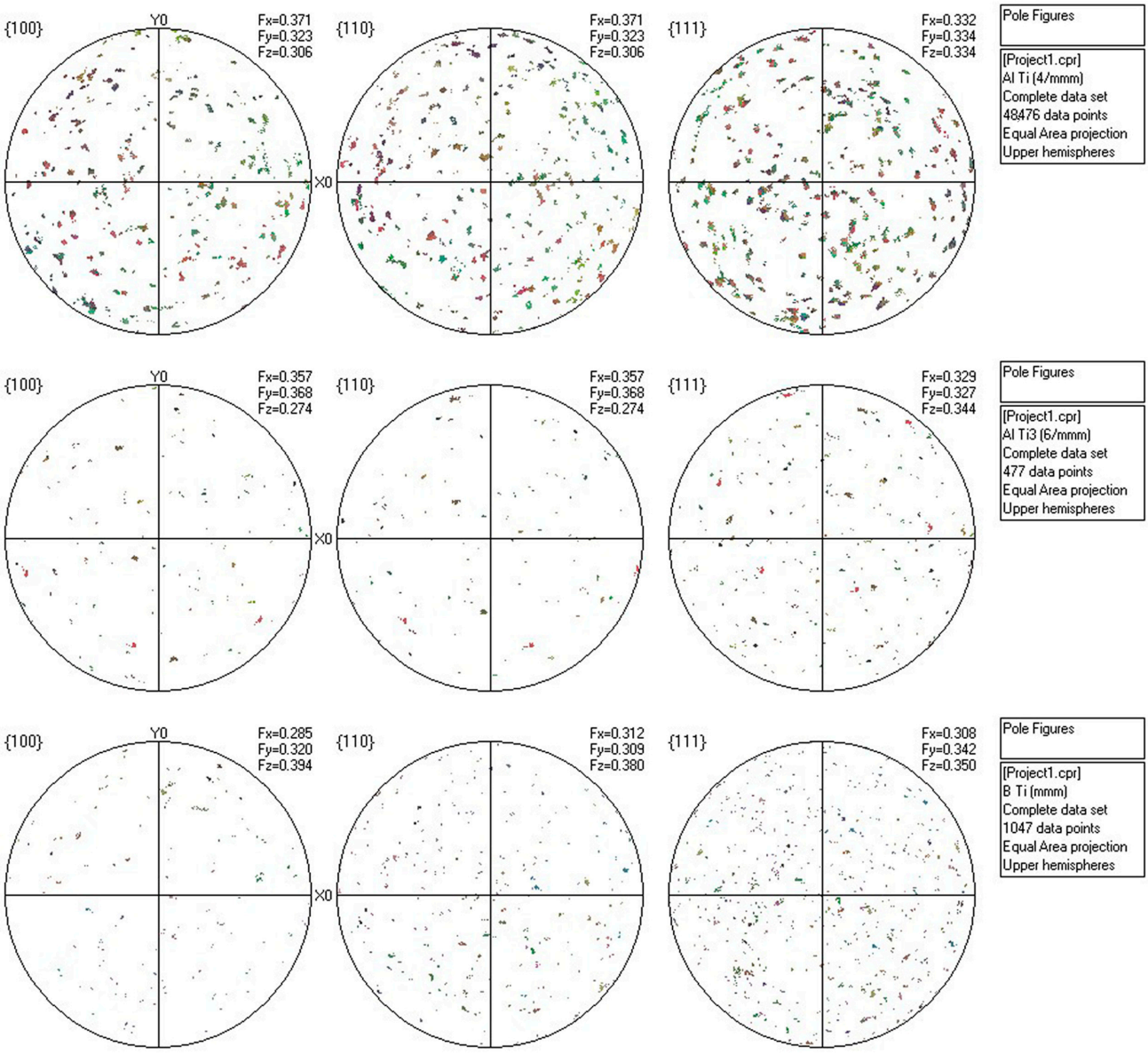

Figure 6. Pole figures of γ, α_2 and TiB phases in Ti-46Al-8Nb-2.5B obtained by EBSD.

3.3. Microstructural Evolution

Microstructures of Ti-46Al-8Nb-*x*B (*x* = 0.7, 1.4, 2.5) alloys after solid solution at 1380 °C followed by water quenching and aging at 900 °C for 3–24 time are shown in Figures 7–9. The Ti-46Al-8Nb-0.7B alloy in Figure 7 shows a gradual coarsening of the matrix lamellar microstructure with an increasing aging time. With the increase in aging time to 12 h, the boride morphology is transformed from a short rod-like dominant in the as-cast alloy to a long curly predominance. And the short bar-shaped borides are also coarsened. Further

increasing the aging time to 24 h, the long curly borides have a tendency to transform into granular borides. This indicates that there is a close relationship between the morphology of borides and heat treatment, and with the increase in aging time, there is an evolution process of boride morphology.

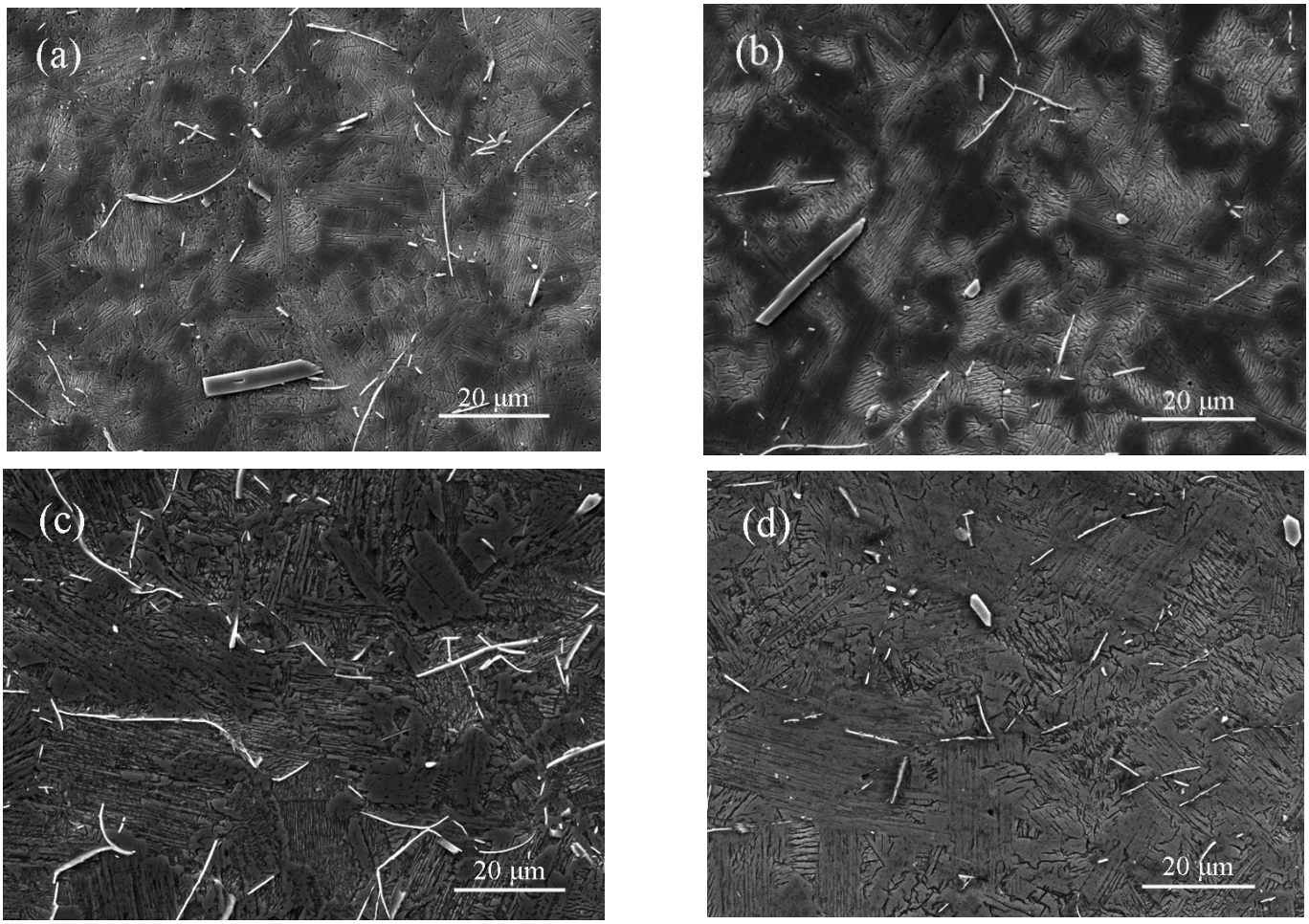

Figure 7. Microstructure of Ti-46Al-8Nb-0.7B alloy after solid solution at 1380 °C followed by water quenching and aging at 900 °C for different time: (**a**) 3 h, (**b**) 6 h, (**c**) 12 h and (**d**) 24 h.

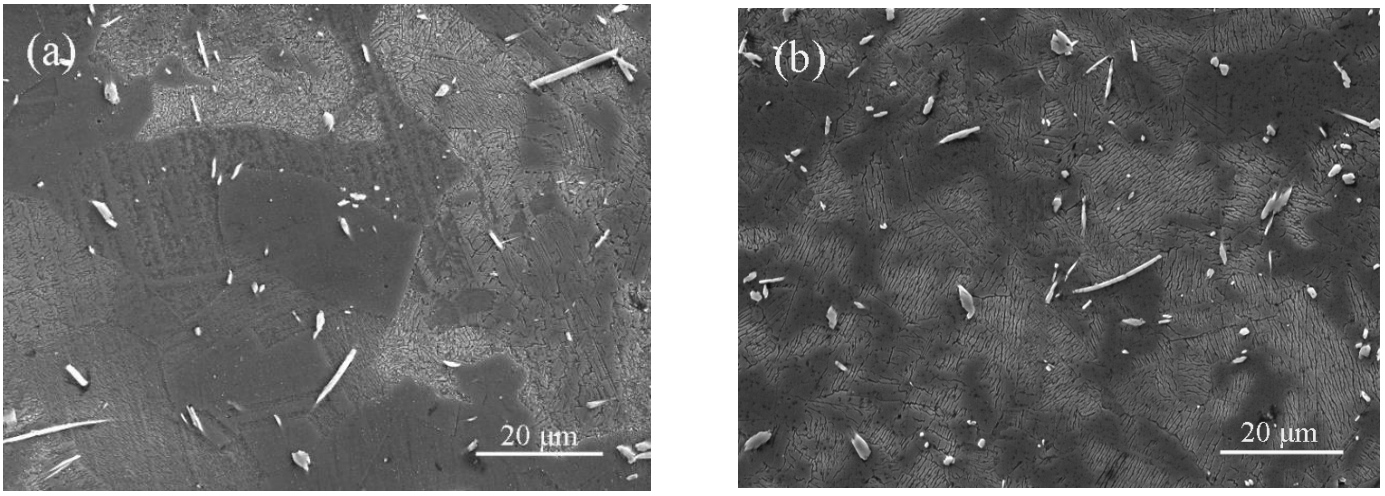

Figure 8. *Cont.*

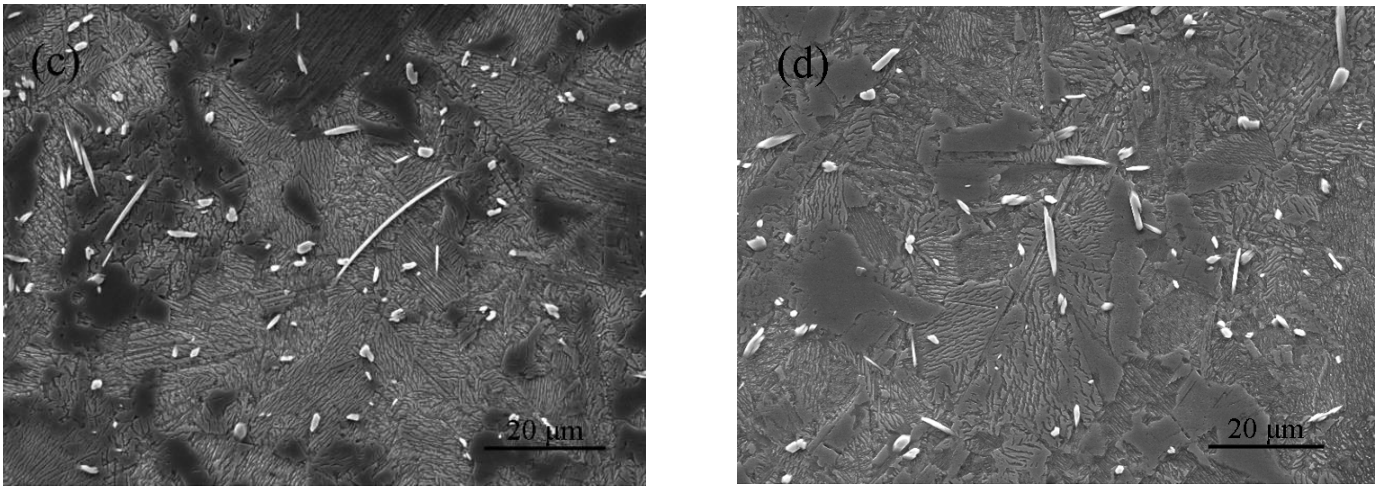

Figure 8. Microstructure of Ti-46Al-8Nb-1.4B alloy after solid solution at 1380 °C followed by water quenching and aging at 900 °C for different time: (**a**) 3 h, (**b**) 6 h, (**c**) 12 h and (**d**) 24 h.

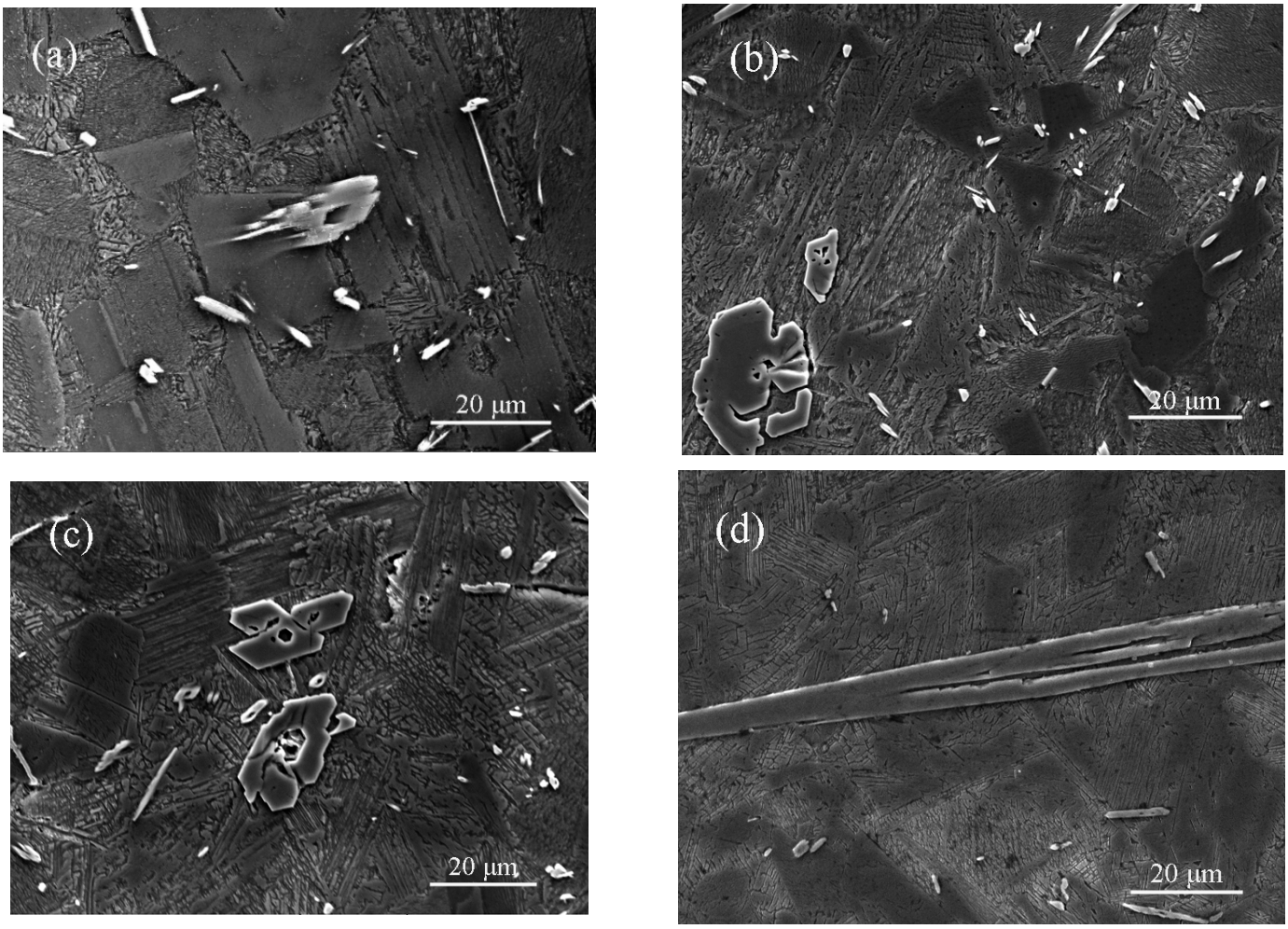

Figure 9. Microstructure of Ti-46Al-8Nb-2.5B alloy after solid solution at 1380 °C followed by water quenching and aging at 900 °C for different time: (**a**) 3 h, (**b**) 6 h, (**c**) 12 h and (**d**) 24 h.

Figure 8 demonstrates the microstructural evolution of Ti-46Al-8Nb-1.4B alloys during heat treatment. For 1.4B alloy, the roughening of the matrix microstructure is not different from that of 0.1B alloy. However, there is a large difference in the boride morphology. With

the increase in aging time, the boride morphology is still dominated by short rods and particles, but all of them are coarsened and grown. In addition, in the 2.5B alloy, as shown in Figure 9, the morphology of the borides has changed to coarse flakes or elongated strips. Significant growth of the borides has occurred. It is clear from the previous analysis that there is a direct relationship between the morphology of the borides and the boron content. The analysis of the heat treatment process shows that the boron content also affects its morphological evolution process during heat treatment.

4. Conclusions

In this work, role of boron addition on the solidification behavior and microstructural evolution during the heat treatment process of a β-solidified high Nb-containing TiAl alloy Ti-46Al-8Nb-xB (x = 0.1, 0.7, 1.4, 2.5 at.%) are investigated. The results show that the solid solubility of the element boron in the experimental alloy is extremely low. Meanwhile, boron can both simultaneously refine the lamellar colony and lamellar microstructure of the alloy. And the reasons for the refining effect of B element are discussed. When the content exceeds its solid solution limit in the alloy, the boron precipitates as a TiB phase of type B27. The morphology of borides is dominated by short rods and granules, and a few morphologies are curly and long. In addition, the presence of borides can become heterogeneous nucleation sites of α phase, which destroys the strict Bragg orientation relationship during the phase transition. As a result, borides significantly weaken the casting texture in the experimental as-cast alloy. During heat treatment, the matrix microstructure of the alloy is gradually coarsened. This work indicates that the morphology of the boride is closely related to the boron content and heat treatment.

Author Contributions: Conceptualization, Z.W. and T.Z.; methodology, Z.W. and T.Z.; software, Y.Z. and Q.L.; validation, X.W.; formal analysis, F.Z. and Y.Z.; investigation, F.Z. and Z.W.; re-sources, X.W. and Q.L.; data curation, F.Z. and Q.L.; writing—original draft preparation, F.Z.; writing—review and editing, Z.W., X.W. and T.Z.; visualization, F.Z.; supervision, Y.Z. and Q.L.; project administration, T.Z.; funding acquisition, Z.W. and Y.Z. All authors have read and agreed to the published version of the manuscript.

Funding: This research was funded by Scientific research project of Education Department of Shaanxi Provincial Government (No. 23JK0293), Shaanxi Natural Science Basic Research Program (No. 2021JQ-808), Doctoral Research Project of Baoji University of Arts and Sciences (No. ZK2018064), Shaanxi Provincial Department of Education Service Local Special Program Project (No. 22JC003), Scientific research project of Education Department of Shaanxi Provincial Government (No. 21JK0482).

Data Availability Statement: The data used in this article have been provided in the paper.

Conflicts of Interest: The authors declare no conflict of interest.

References

1. Yao, J.; Fan, S.; Liu, X.; Ding, X.; Huang, H.; Wu, W.; Wang, Q.; Wang, L.; Su, Y. Pollution-free grain refinement of cast TiAl alloys by vacuum mechanical vibration solidification. *Mater. Sci. Eng. A* **2023**, *865*, 144630. [CrossRef]
2. Park, J.; Yang, G.; Kim, S. A high tensile strength above 900 °C in β-solidified TiAl alloy through alloy design and microstructure optimization. *J. Alloys Compd.* **2023**, *947*, 169676. [CrossRef]
3. Sun, T.; Guo, Z.; Cao, J.; Liang, Y.; Lin, J. Isothermal oxidation behavior of high-Nb-containing TiAl alloys doped with W, B, Y, and C/Si. *Corros. Sci.* **2023**, *213*, 110980. [CrossRef]
4. Zhao, X.; Wei, J.; Niu, H.; Cao, S.; Du, Z.; Jia, Y.; Yao, H.; Zhang, Z.; Han, J. Mechanical and physical characterizations of a three-Phase TiAl alloy during near isothermal forging. *Crystals* **2022**, *12*, 1391. [CrossRef]
5. Abdo, H.; Abdus, S.; Mohammed, J.; Ragab, S.; Seikh, A. Mitigating Corrosion Effects of Ti-48Al-2Cr-2Nb Alloy Fabricated via Electron Beam Melting (EBM) Technique by Regulating the Immersion Conditions. *Crystals* **2021**, *11*, 889. [CrossRef]
6. Liu, S.; Ding, H.; Chen, R.; Guo, J.; Fu, H. Evolution of rapidly grown cellular microstructure during heat treatment of TiAl-based intermetallic and its effect on micromechanical properties. *Intermetallics* **2021**, *132*, 107166. [CrossRef]
7. Adachi, K.; Waki, H. Elastic constants and internal friction of forged β-solidifying TiAl alloys at room temperature and high temperature. *Intermetallics* **2022**, *142*, 107456. [CrossRef]
8. Huang, L.; Geng, L.; Peng, H. Strengthening and Toughening Mechanisms of the Second Phase in Titanium Alloys and Titanium Matrix Composites. *Mater. China* **2019**, *3*, 214–222.

9. Xu, R.R.; Li, H.; Li, M.Q. Flow softening mechanism in isothermal compression of β-solidifying γ-TiAl alloy. *Mater. Des.* **2020**, *186*, 108328. [CrossRef]
10. Huang, D.; Zhou, Y.; Yao, X.; Tan, Q.; Chang, H.; Wang, D.; Lu, S.; Liu, S.; Xu, J.; Jin, S.; et al. From crack-prone to crack-free: Unravelling the roles of LaB6 in a β-solidifying TiAl alloy fabricated with laser additive manufacturing. *Mater. Sci. Eng. A* **2022**, *861*, 144358. [CrossRef]
11. Wang, L.; Shen, C.; Zhang, Y.; Li, F.; Huang, Y.; Ding, Y.; Xin, J.; Zhou, W.; Hua, X. Effect of Al content on the microstructure and mechanical properties of γ-TiAl alloy fabricated by twin-wire plasma arc additive manufacturing system. *Mater. Sci. Eng. A* **2021**, *826*, 142008. [CrossRef]
12. Zhang, F.; Wu, Z.; Zhang, T.; Hu, R.; Wang, X. Microstructure Sensitivity on Environmental Embrittlement of a High Nb Containing TiAl Alloy under Different Atmospheres. *Materials* **2022**, *15*, 8508. [CrossRef] [PubMed]
13. Niu, H.; Chen, X.; Chen, Y.; Zhao, S.; Liu, G.; Zhang, D. Microstructural stability, phase transformation and mechanical properties of a fully-lamellar microstructure of a Mo-modified high-Nb γ-TiAl alloy. *Mater. Sci. Eng. A* **2020**, *784*, 139313. [CrossRef]
14. Kim, J.; Park, E.; Lee, T.; Ryu, S.; Kim, S.; Kim, S. Origin of enhanced room temperature ductility in TiAl alloys: Reducing activation difference of deformation mechanism of γ phase. *J. Alloys Compd.* **2022**, *899*, 163307. [CrossRef]
15. Wang, Q.; Chen, R.; Yang, Y.; Guo, J.; Su, Y.; Ding, H.; Fu, H. Effects of V and B, Y additions on the microstructure and creep behaviour of high-Nb TiAl alloys. *J. Alloys Compd.* **2018**, *747*, 640–647. [CrossRef]
16. Zhang, T.; Wu, Z.; Hu, R.; Zhang, F.; Kou, H.; Li, J. Influence of nitrogen on the microstructure and solidification behavior of high Nb containing TiAl alloys. *Mater. Des.* **2016**, *103*, 100–105. [CrossRef]
17. Fang, H.; Zhou, L.; Wang, S.; Chen, R.; Xu, Q.; Yan, Y.; Guo, J. Formation and kinds of boride on microstructure evolution and mechanical properties in Ti47.5Al2.0Cr2.0NbxB alloys. *Intermetallics* **2022**, *141*, 107427. [CrossRef]
18. Tan, Y.; Chen, R.; Fang, H.; Liu, Y.; Cui, H.; Su, Y.; Guo, J.; Fu, H. Enhanced strength and ductility in Ti46Al4Nb1Mo alloys via boron addition. *J. Mater. Sci. Technol.* **2022**, *102*, 16–23. [CrossRef]
19. Yang, C.; Hu, D.; Huang, A.; Dixon, M. Solidification and grain refinement in Ti45Al2Mn2Nb1B subjected to fast cooling. *Intermetallics* **2013**, *32*, 64–71. [CrossRef]
20. Oehring, M.; Stark, A.; Paul, J.D.H.; Lippmann, T.; Pyczak, F. Microstructural refinement of boron-containing β-solidifying γ-titanium aluminide alloys through heat treatments in the β phase field. *Intermetallics* **2013**, *32*, 12–20. [CrossRef]
21. Witusiewicz, T.; Bondar, A.; Hecht, U. Velikanova Ya: The Al-B-Nb-Ti system: IV. Experimental study and thermodynamic re-evaluation of the binary Al-Nb and ternary Al-Nb-Ti systems. *J. Alloys Compd.* **2009**, *472*, 133–161. [CrossRef]
22. Schwaighofer, E.; Rashkova, B.; Clemens, H.; Stark, A.; Mayer, S. Effect of carbon addition on solidification behavior, phase evolution and creep properties of an intermetallic β-stabilized γ-TiAl based alloy. *Intermetallics* **2014**, *46*, 173–184. [CrossRef]
23. Zhu, H.; Wei, T.; Blackford, M.; Short, K.; Carr, D.; Harrison, R.; Edwards, L.; Seo, D.; Maruyama, K. Irradiation behaviour of α_2 and γ phases in He ion implanted titanium aluminide alloy. *Intermetallics* **2014**, *50*, 28–33. [CrossRef]
24. Wu, Z.; Hu, R.; Zhang, T.; Zhang, F.; Kou, H.; Li, J. Understanding the role of carbon atoms on microstructure and phase transformation of high Nb containing TiAl alloys. *Mater. Charact.* **2017**, *124*, 1–7. [CrossRef]
25. Ouadah, O.; Merad, G.; Abdelkader, H.S. Energetic segregation of B, C, N, O at the γ-TiAl/α_2-Ti_3Al interface via DFT approach. *Vacuum* **2021**, *186*, 110045. [CrossRef]
26. Kartavykh, A.; Gorshenkov, M.; Tcherdyntsev, V.; Podgorny, D. On the state of boride precipitates in grain refined TiAl-based alloys with high Nb content. *J. Alloys Compd.* **2014**, *586*, S153–S158. [CrossRef]
27. Hu, D. Effect of composition on grain refinement in TiAl-based alloys. *Intermetallics* **2001**, *9*, 1037–1043. [CrossRef]
28. Hecht, U.; Witusiewicz, V.; Drevermann, A.; Zollinger, J. Grain refinement by low boron additions in niobium-rich TiAl-based alloys. *Intermetallics* **2008**, *16*, 969–978. [CrossRef]
29. Yang, C.; Jiang, H.; Hu, D.; Huang, A.; Dixon, M. Effect of boron concentration on phase transformation texture in as-solidified Ti44Al8NbxB. *Scr. Mater.* **2012**, *67*, 85–88. [CrossRef]
30. Liu, B.; Liu, L.; Xing, W.; Liu, R.; Yang, R.; Withey, P.; Zhu, J.; Yu, R. Structural stability and the alloying effect of TiB polymorphs in TiAl alloys. *Intermetallics* **2017**, *90*, 97–102. [CrossRef]
31. Hu, D. Role of boron in TiAl alloy development: A review. *Rare Met.* **2016**, *35*, 1–14. [CrossRef]